

AD-A108 363

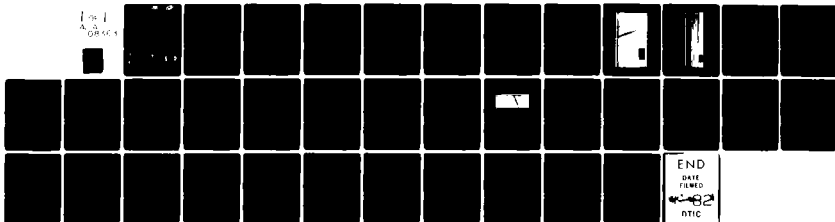
NAVAL RESEARCH LAB WASHINGTON DC
WEAK AND STRONG IGNITION. I. NUMERICAL SIMULATIONS OF SHOCK TUB--ETC(U)
DEC 81 E S ORAN; T R YOUNG; J P BORIS
NRL-MR-4664

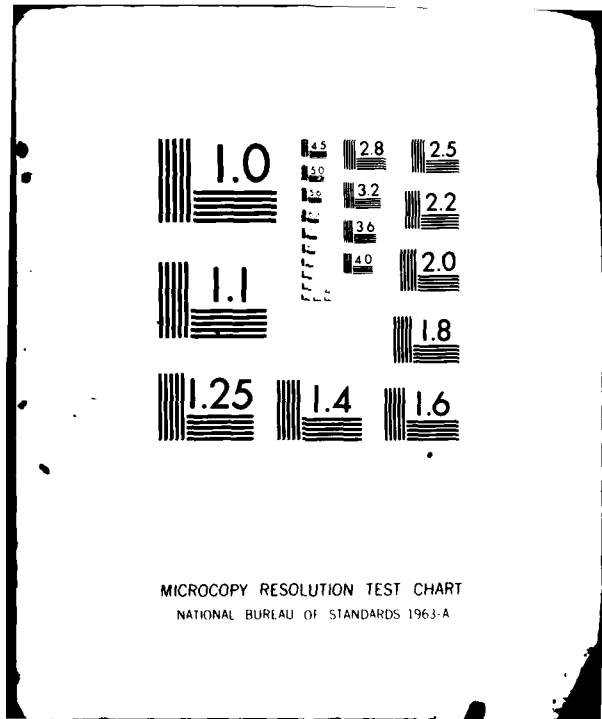
F/G 21/2

UNCLASSIFIED

NL

1 of 1
pages





MICROCOPY RESOLUTION TEST CHART
NATIONAL BUREAU OF STANDARDS 1963-A

AD A103303

37

Weak and Strong Ignition I. Numerical Simulations of Shock Tube Experiments

E. S. ORAN, T. R. YOUNG AND J. P. BORN

Laboratory for Computational Physics

A. COHEN

*Ballistics Research Laboratory
Aberdeen, MD.*

December 7, 1981



NAVAL RESEARCH LABORATORY
Washington, D.C.

Approved for public release; distribution unlimited.

81 12 10 006

DTIC
ELECTE
DEC 10 1981
S D D

THIS FILE COPY

REPORT DOCUMENTATION PAGE		READ INSTRUCTIONS BEFORE COMPLETING FORM
1. REPORT NUMBER NRL Memorandum Report 4664	2. GOVT ACCESSION NO. AD-A108	3. RECIPIENT'S CATALOG NUMBER 363
4. TITLE (and Subtitle) WEAK AND STRONG IGNITION I. NUMERICAL SIMULATIONS OF SHOCK TUBE EXPERIMENTS	5. TYPE OF REPORT & PERIOD COVERED Interim report on a continuing NRL problem.	
	6. PERFORMING ORG. REPORT NUMBER	
7. AUTHOR(s) E.S. Oran, T.R. Young, J.P. Boris and A. Cohen*	8. CONTRACT OR GRANT NUMBER(s)	
9. PERFORMING ORGANIZATION NAME AND ADDRESS Naval Research Laboratory Washington, DC 20375	10. PROGRAM ELEMENT, PROJECT, TASK AREA & WORK UNIT NUMBERS RR0130144 & ZF43451001; 44-0572-01 & 44-0061-A1	
11. CONTROLLING OFFICE NAME AND ADDRESS Office of Naval Research Washington, DC 22217	12. REPORT DATE December 7, 1981	
	13. NUMBER OF PAGES 36	
14. MONITORING AGENCY NAME & ADDRESS (if different from Controlling Office)	15. SECURITY CLASS. (of this report) UNCLASSIFIED	
	15a. DECLASSIFICATION/DOWNGRADING SCHEDULE	
16. DISTRIBUTION STATEMENT (of this Report) Approved for public release; distribution unlimited.		
17. DISTRIBUTION STATEMENT (of the abstract entered in Block 20, if different from Report)		
18. SUPPLEMENTARY NOTES *Present address: Ballistics Research Laboratory, Aberdeen, MD.		
19. KEY WORDS (Continue on reverse side if necessary and identify by block number) Combustion Shock tubes Detonations Hydrogen-oxygen combustion		
20. ABSTRACT (Continue on reverse side if necessary and identify by block number) Detailed one-dimensional calculations have been performed to simulate weak and strong ignition in reflected shock tube experiments in hydrogen-oxygen-argon mixtures. It is found that the experiment and simulations agree well in the strong ignition case studied. In the weak ignition case, the simulations show the same qualitative behavior as the experiment. Here ignition starts at a distance away from the reflecting wall at a time much earlier than the calculated chemical induction time. This latter effect is shown to (Continues)		

DD FORM 1473
1 JAN 73

EDITION OF 1 NOV 65 IS OBSOLETE
S. N. 0102-014-6601

SECURITY CLASSIFICATION OF THIS PAGE (When Data Entered)

21-1

20. ABSTRACT (Continued)

arise because of the sensitivity of the chemical induction time to fluctuations in the calculation. In the calculations these fluctuations arise from small numerical inaccuracies. In experiments, they can arise from a number of sources including nonuniformities in the incident shock wave leading to non-uniform reflection, thermal conduction to the walls, and interactions with boundary layers.

CONTENTS

I. INTRODUCTION	1
II. THE EXPERIMENTS	2
III. THE NUMERICAL MODEL	8
IV. SIMULATION OF THE STRONG IGNITION EXPERIMENT	14
V. SIMULATION OF A WEAK IGNITION CASE	20
VI. DISCUSSION	29
ACKNOWLEDGEMENTS	30
REFERENCES	31

Accession For	
NTIS GRA&I	<input checked="" type="checkbox"/>
DTIC TAB	<input type="checkbox"/>
Unannounced	<input type="checkbox"/>
Justification	
By _____	
Distribution/	
Availability Codes	
Dist	Avail and/or Special
A	

WEAK AND STRONG IGNITION
I. NUMERICAL SIMULATIONS OF SHOCK TUBE EXPERIMENTS

I. Introduction

Anomalously low and somewhat erratic ignition temperatures in mixtures of hydrogen and oxygen were first reported by a number of authors doing shock tube or adiabatic compression experiments [1,2,3,4]. Later the work of Strehlow and Soloukhin and their coworkers [5,6,7,8,9,10] described variations in the ignition behavior of mixtures ignited behind reflected shocks. Strehlow catalogued three types of behavior behind the reflected shock: (1) acceleration of a reflected shock when a pressure wave generated by released chemical energy reaches the reflected shock; (2) an accelerating wave headed by a shock behind the reflected wave; and (3) a fast release of energy leading to a detonation behind the reflected wave. Voevodsky and Soloukhin [10], who concentrated on variations in ignition due to chemical kinetics, defined two ignition regimes separated by an extended second explosion limit. "Strong" or "sharp" ignition was said to occur when the results of schlieren streak photographs showed that a single ignition locus at the reflecting wall was sufficient to form a detonation front. "Mild" or "weak" ignition occurred at lower temperatures where the reaction was initiated at many loci which finally merge together to form a uniform front.

The work of Meyer and Oppenheim [11] showed that mild ignition started in distinct centers in the shock tube, usually in stagnant corners. They then showed that the chemical induction time can be very sensitive to temperature variations which occur due to nonuniformities behind shock waves. Subsequently they developed a "coherence" theory for ignition which gave criteria for strong ignition based on a sufficiently high rate of chemical energy release in a large enough radius

Manuscript submitted September 15, 1981.

[12,13]. Properties of these "ignition kernals" or "exothermic centers" were described by Zajac and Oppenheim [14], van Tiggelen [15] and Borisov [16]. Borisov described the origins of the exothermic centers as resulting from temperature fluctuations, fluctuations is activated molecules or radicals, pressure waves, or catalytic generation of radicals on suspended particles. He pointed out that it is virtually impossible to eliminate turbulence and pressure waves due to non-uniformities in temperature and concentration. These fluctuations cause the induction times of reactive mixtures to vary in time and space.

In this paper we use data from shock tube experiments by Cohen and Larsen [17] combined with numerical simulations to study weak and strong ignition. As Borisov suggested, we find that the weak ignition system is extremely sensitive to small acoustic perturbations. In these cases, the detailed one-dimensional simulations described below show fluctuation behavior quite similar to that seen in the multi-dimensional experiments. When the systems are not as sensitive, as in the strong ignition case, we find using a previously validated set of rate constants, that the simulations and the experiment are in excellent quantitative agreement.

II. The Experiments

The calculations described in this paper are based on two of a series of reflected shock tube experiments performed by Cohen and Larsen [17]. The experimental technique consisted of simultaneous measurements of pressure, UV light transmission (either emission or a combination of emission plus absorption), and recording through time resolved schlieren photography of the shock reflection-reaction wave formation process. The shock tube and technique for taking time-resolved schlieren photographs have been described by Strehlow and Cohen [15]. Pressure was

measured by a fast response piezoelectric transducer (3 μ sec risetime) flush mounted at the center of the end wall of the shock tube. The transducer signal was recorded by means of an amplifier (Kistler Model 565) and an oscilloscope. Another pressure transducer was located 198 mm upstream from the back wall, primarily as a trigger for oscilloscopes and counters.

For the light transmission measurements, a monochromator (Schoeffel Model QPM30) was used to isolate a region centered at 3100° A (theoretical half band width = 50° A). A photomultiplier (1P28) monitored the transmitted UV light intensity. The effective absorption path is restricted to a region 1 mm from the back wall and 1 mm wide by slits located on the monochromator and the shock tube window. The signal was recorded by means of a cathode follower and oscilloscope. The risetime of the electronic circuits was less than 1 μ sec. Figure 1 contains a schematic diagram of the experimental arrangement.

The typical experimental cases will be studied in detail using the model described below. One set of initial conditions is in the strong ignition limit and the data is compared directly to the results of a simulation. The other experimental conditions are in the "mild" or "weak" ignition limit. Because the timescales for this latter case are relatively long, the cost of a simulation of these exact parameters is correspondingly high. Thus we have simulated a problem which is still in the weak ignition limit, but the temperature and pressure have been raised slightly. The results of the simulation are then used to guide the interpretation of the experiment. Figures 2 and 3 show the schlieren photographs for the experimental parameters described in Tables 1 and 2.

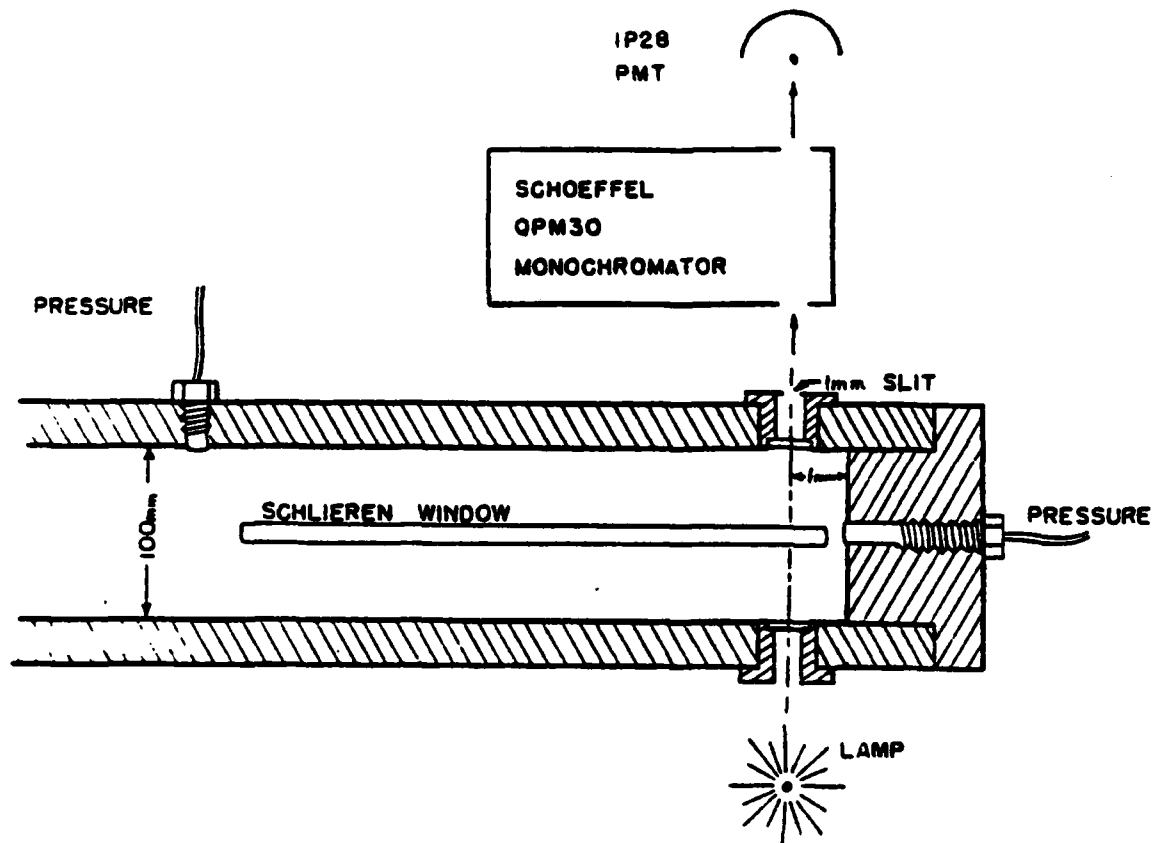


Fig. 1 - Schematic diagram of the shock tube instrumentation

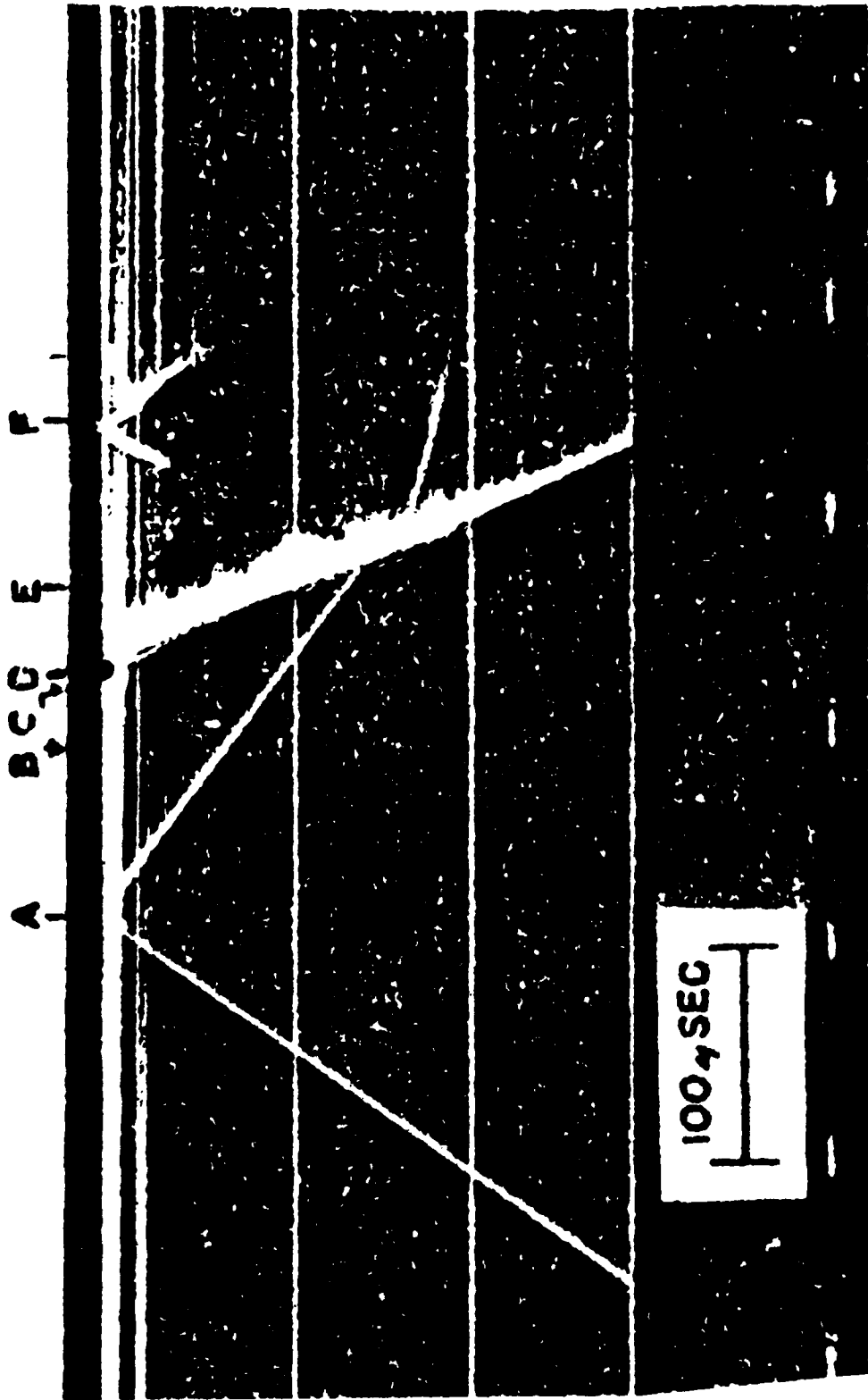


Fig. 2 — Schlieren record of strong ignition case: A) shock reflection at the wall, B) initial absorption signal at slit 1 mm from the reflecting wall, C) initial emission pulse, D) reaction wave formation at the reflecting wall, E) second emission pulse, and F) peak absorption



Fig. 3 — Schlieren record of weak ignition case: A) shock reflection at wall, B) initial absorption signal at slit 1 mm from the reflecting wall, C) maximum absorption signal 1 mm from reflecting wall, D) reaction wave formation at the reflecting wall, E) initial pressure increase at the reflecting wall

Table I

Parameters for the Strong Ignition Experiment

H₂:O₂:Ar/2:1:7

	<u>Undisturbed</u>	<u>Incident</u>	<u>Reflected</u>
Temperature	298 K	621 K	1036 K
Pressure	0.066 atm	0.362 atm	1.3 atm
Fluid Velocity		4.76x10 ⁴ cm/sec	
Shock Velocity		7.54x10 ⁴ cm/s	4.5x10 ⁴ cm/s
Mach Number		2.165	

Table II

Parameters for the Weak Ignition Experiment

H₂:O₂:Ar/8:2:90

	<u>Undisturbed</u>	<u>Incident</u>	<u>Reflected</u>
Temperature	298 K	601 K	972 K
Pressure	0.233 atm	1.07 atm	3.4 atm
Fluid Velocity		3.74x10 ⁴ cm/s	
Shock Velocity		6.59x10 ⁴ cm/s	4.36x10 ⁴
Mach Number		1.98	

III. The Numerical Model

The conservation equations for mass, momentum and energy [18] solved in the calculations performed below may be written

$$\frac{\partial \rho}{\partial t} = - \nabla \cdot \rho \underline{v} \quad (1)$$

$$\frac{\partial n_j}{\partial t} = - \nabla \cdot n_j \underline{V}_j - \nabla \cdot n_j \underline{v} + Q_j - L_j n_j \quad (2)$$

$$\frac{\partial(\rho \underline{v})}{\partial t} = - \nabla \cdot (\rho \underline{v} \underline{v}) - \nabla P \quad (3)$$

$$\frac{\partial \mathcal{E}}{\partial t} = - \nabla \cdot \underline{E} \underline{v} - \nabla \cdot P \underline{v} - \nabla \cdot \underline{Q} \quad (4)$$

where the heat flux, \underline{Q} , is defined as

$$\underline{Q} = - \lambda \nabla T + \sum_j n_j h_j \underline{V}_j \quad (5)$$

The quantities ρ , $\rho \underline{v}$, \mathcal{E} and P are the total mass, momentum, energy density, and pressure, respectively. Here \underline{v} is the fluid velocity, and k_B is Boltzmann's constant. The $\{n_i\}$ and $\{\underline{V}_i\}$ are the number density and the diffusion velocities of the individual chemical species. The quantity λ is the thermal conductivity coefficient of the gas mixture at specified $\{n_j\}$ and temperature, T . The $\{Q_j\}$ and $\{L_j\}$ refer to chemical production and loss processes for species j . The last term in Equation (5) represents the local change in energy due to molecular diffusion and chemical reactions which must be added to the fluid dynamic energy density. The quantities $\{h_j\}$ are the temperature dependent enthalpies for each species. We note that viscosity and thermal diffusion have been omitted from Equations (1)-(5) since they have a negligible effect on the solutions presented below.

The reactive shock model used to perform the calculations described below solves these equations in one spatial dimension for the generalized coordinate, r . Though r may represent position in either cartesian, cylindrical spherical or some generalized coordinates, the particular application here is in cartesian geometry. The ideal gas law is assumed so that

$$P = Nk_B T \quad . \quad (6)$$

where N is the total number density,

$$N = \sum_j n_j \quad . \quad (7)$$

Thus, we may write the internal energy per unit volume as

$$\epsilon = \sum_j n_j h_n - P = H - P \quad (8)$$

The internal energy is related to the pressure and total energy by

$$\epsilon = \frac{P}{\gamma-1} = \epsilon - \frac{1}{2} \rho v^2 - \sum_j h_{oj} n_j \equiv E - \frac{1}{2} \rho v^2 \quad (9)$$

where γ is the ratio of specific heats, $\{h_{oj}\}$ is the set of heats of formation at 0°K of the species j , and E is the total energy minus the total heat of formation. The diffusion velocities $\{V_j\}$ are found by inverting the following matrix equations [18, 19]:

$$S_j = \sum_k \frac{n_j n_k}{N^2 D_{jk}} (v_k - v_j) \equiv \sum_k W_{jk} (v_k - v_j) \quad , \quad (10)$$

subject to the constraint

$$\sum_j \rho_j V_j = 0 \quad . \quad (11)$$

The source terms S_j are defined as

$$S_j \equiv \bar{v} (n_j/N) - (\rho_j/\rho - n_j/N) \frac{VP}{P} - \sum_k \frac{n_j n_k}{N^2 D_{jk}} (D_k^T/\rho_k - D_j^T/\rho_j) \frac{VT}{T} \quad .(12)$$

Throughout this paper physical quantities are generally give in cgs K units although pressure is also given in atmosphere.

The convective and diffusive transport terms in Equations (1)-(4) are solved separately and then coupled together by timestep splitting with asymptotics as described by Oran and Boris [18]. The convection terms are solved using one variant of the Flux-Corrected Transport (FCT) method [20,21]. This is a conservative, monotonic algorithm with fourth order accuracy which does not require artificial viscosity to stabilize shocks. The ordinary differential equations describing the chemical kinetics are represented by the Q_j and the $L_j n_j$ terms in Equation (2). These are solved using VSAIM, a version of the CHEMEQ algorithm [22,23], which has been specially optimized for use in dynamic models. For most of the calculations presented below the timescales under consideration are short and the diffusive transport processes, thermal conduction and molecular diffusion, have negligible effect. Thus the calculations performed omit these processes unless otherwise indicated.

The detailed simulations of the shock tube experiments require that we generalize the adaptive gridding method used previously [24] to include two finely gridded regions. The first region moves with the shock front, surrounding first the incident and then reflected shock front. The second region stays at the reflecting wall until the reaction wave has developed and then moves with the reaction wave. Each region may have a different minimum computational cell size. When the shock and reaction waves merge, the detonation front then maintains the cell size characteristic of the most finely zoned region. For many of the calculations presented below, computational cell sizes varied nearly two orders of magnitude from the most finely zoned region around the reaction wave to the coarsest zoning in the calculation.

Figure 4 shows the geometry and general configuration of the calculations used to simulate the experiments. The calculation is done in Cartesian geometry and initialized with an incident shock moving from right to left. The left hand boundary is a reflecting wall, and the right hand boundary condition ensures that there is a constant inflow of material moving at the incident shock velocity. We thus minimized computational costs by not modelling the full problem which includes a driver section of the shock tube. This is valid because throughout the calculated time span the reflected shock wave remains well separated from the contact discontinuity formed when the diaphragm initially burst.

The chemical kinetics rate scheme used consists of about fifty chemical rates relating the species H_2 , O_2 , O , H , OH , HO_2 , H_2O_2 , and H_2O . It has been tested extensively against experimental data [25, 26, 27, 28] and shown to give excellent results. Recent calculations have shown that it also gives values of the flame velocity which compare well with experimental measurements. The reaction rate scheme is give in Table 3. Heats of formation and enthalpies have been taken from the JANAF tables [29].

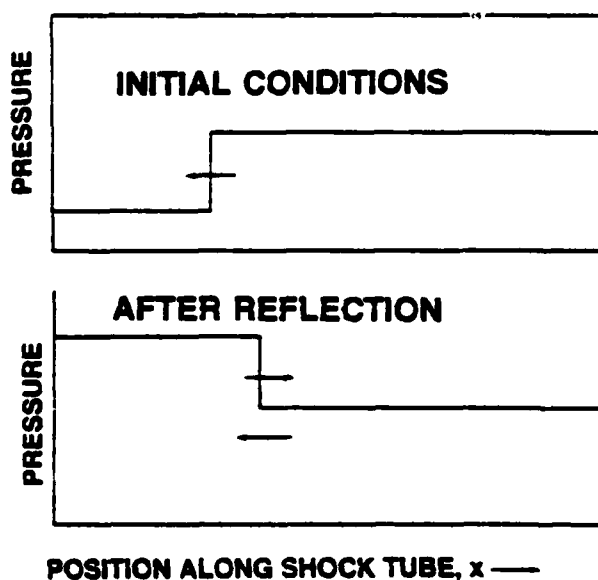


Fig. 4 — Schematic of the geometry used in the calculations

Table III. H₂-O₂ Elementary Reactive Mechanism

Reaction	$k_1 = AT^B \exp(-C/T)^{(a)}$			Reference
	A ^(b)	B	C ^(b)	
H + HO \rightleftharpoons O + H ₂	1.40(-14) 3.00(-14)	1.00 1.00	3.50(+03) 4.48(+03)	[33] [33]
H + HO ₂ \rightleftharpoons H ₂ + O ₂	4.20(-11) 9.10(-11)	0.00 0.00	3.50(+02) 2.91(+04)	[33] [33]
H + HO ₂ \rightleftharpoons HO + HO	4.20(-10) 2.00(-11)	0.00 0.00	9.50(+02) 2.02(+04)	[33] [33]
H + HO ₂ \rightleftharpoons O + H ₂ O	8.30(-11) 1.75(-12)	0.00 0.45	5.00(+02) 2.84(+04)	[34] $k_r = k_f/K_c$
H + H ₂ O ₂ \rightleftharpoons HO ₂ + H ₂	2.80(-12) 1.20(-12)	0.00 0.00	1.90(+03) 9.40(+03)	[33] [33]
H + H ₂ O ₂ \rightleftharpoons HO + H ₂ O	5.28(-10) 3.99(-10)	0.00 0.00	4.50(+03) 4.05(+04)	[33] $k_r = k_f/K_c$
HO + H ₂ \rightleftharpoons H + H ₂ O	1.83(-15) 1.79(-14)	1.30 1.20	1.84(+03) 9.61(+03)	[35] [35]
HO + HO \rightleftharpoons H ₂ + O ₂	1.09(-13) 2.82(-11)	0.26 0.00	1.47(+04) 2.42(+04)	$k_f = k_r/K_c$ [36]
HO + HO \rightleftharpoons O + H ₂ O	1.00(-16) 3.20(-15)	1.30 1.16	0.00(+00) 8.77(+03)	[35] $k_r = k_f/K_c$
HO + HO ₂ \rightleftharpoons H ₂ O + O ₂	8.30(-11) 2.38(-10)	0.00 0.17	5.03(+02) 3.69(+04)	[37] $k_r = k_f/K_c$
HO + H ₂ O \rightleftharpoons HO ₂ + H ₂	1.70(-11) 4.70(-11)	0.00 0.00	9.10(+02) 1.65(+04)	[33] [33]
HO + O ₃ \rightleftharpoons HO ₂ + O ₂	1.60(-12) 6.69(-14)	0.00 0.33	9.56(+02) 2.04(+04)	[34] $k_r = k_f/K_c$
HO + H ₂ \rightleftharpoons HO + H ₂ O	1.20(-12) 1.33(-14)	0.00 0.43	9.41(+03) 3.62(+04)	[36] $k_r = k_f/K_c$
HO ₂ + HO ₂ \rightleftharpoons H ₂ O ₂ + O ₂	3.00(-11) 1.57(-09)	0.00 -0.38	5.00(+02) 2.20(+04)	[34] $k_r = k_f/K_c$

Table III. (continued)
 H_2-O_2 Elementary Reactive Mechanism

Reaction	$k_i = AT^B \exp(-C/T)^{(a)}$			Reference
	A ^(b)	B	C ^(b)	
$O + HO \rightleftharpoons H + O_2$	2.72(-12) 3.70(-10)	0.28 0.00	-8.10(+01) 8.45(+03)	$k_f = k_r/K_c$ [33]
$O + HO_2 \rightleftharpoons HO + O_2$	8.32(-11) 2.20(-11)	0.00 0.18	5.03(+02) 2.82(+04)	[37] $k_r = k_f/K_c$
$O + H_2O_2 \rightleftharpoons H_2O + O_2$	1.40(-12) 5.70(-14)	0.00 0.52	2.12(+03) 4.48(+04)	[34] $k_r = k_f/K_c$
$O + H_2O_2 \rightleftharpoons HO + HO_2$	1.40(-12) 2.07(-15)	0.00 0.64	2.13(+03) 8.23(+03)	[34] $k_r = k_f/K_c$
$H + H + M \rightleftharpoons H_2 + M$	1.80(-30) 3.70(-10)	-1.00 0.00	0.00(+00) 4.83(-04)	[33] [33]
$H + HO + M \rightleftharpoons H_2O + M$	6.20(-26) 5.80(-09)	-2.00 0.00	0.00(+00) 5.29(+04)	[33] [33]
$H + O_2 + M \rightleftharpoons HO_2 + M$	4.14(-33) 3.50(-09)	0.00 0.00	-5.00(+02) 2.30(+04)	[33] [33]
$HO + HO + M \rightleftharpoons H_2O_2 + M$	2.50(-33) 2.00(-07)	0.00 0.00	-2.55(+03) 2.29(+04)	[33] [33]
$O + H + M \rightleftharpoons HO + M$	8.28(-29) 2.33(-10)	-1.00 0.21	0.00(+00) 5.10(+04)	[38] $k_r = k_f/K_c$
$O + HO + M \rightleftharpoons HO_2 + M$	2.80(-31) 1.10(-04)	0.00 -0.43	0.00(+00) 3.22(+04)	[38] $k_r = k_f/K_c$
$O + O + M \rightleftharpoons O_2 + M$	5.20(-35) 3.00(-06)	0.00 -1.00	-9.00(+02) 5.94(+04)	[33] [33]

(a) Bimolecular reaction rate constants are given in units of $cm^3/(molecule \text{ sec})$.
 Termolecular reaction rate constants are given in units of $cm^6/(molecule^2 \text{ sec})$.

(b) Exponentials to the base 10 are given in parenthesis; i.e., 1.00(-10) = 1.00×10^{-10} .

IV. Simulation of the Strong Ignition Experiment

The initial calculations performed tested the individual chemical and hydrodynamics algorithms separately [30]. First we performed a purely chemical kinetic calculation to determine the induction time of a mixture of $H_2:O_2:Ar/2:1:7$ at the reflected shock temperature and pressure. Figure 5 shows a series of a constant volume adiabatic calculations performed for various initial temperatures using the CHEMEQ algorithm. The induction time for the purpose of this paper is defined as that time at which the temperature increases just 20 K from its initial value. As can be seen from the figure, the induction time at 1034K is 109 ± 1 usec, in good agreement with the times as measured by the shock tube experiment. Similarly, tests of the hydrodynamics algorithm alone also give shock velocities in agreement with experiment. Thus we know that the individual chemical and hydrodynamic parts of the model are correct. The next step is then to use the model to study the interaction of these processes in the reactive flow.

One problem with numerical simulation even in one dimension is interpreting the large quantity of output data. At each timestep we calculate mass, momentum, energy, temperature, and a number of species densities. In order to compare the simulation most effectively with the experiment, we have chosen to follow the time-dependent behavior of two quantities: the maximum pressure in the system modelled and the fluid velocity at the reflecting wall. The maximum pressure at each timestep is constant until the incident shock is reflected; then it jumps to a higher value. It increases again when chemical energy is released and the reaction wave starts, and reaches a maximum at the time when the reaction wave and reflected shock wave merge. The fluid velocity behind the reflected shock in the ideal case is zero. In the simulation it is zero until the incident shock hits the wall. At this point it oscillates wildly to maximum values of nearly

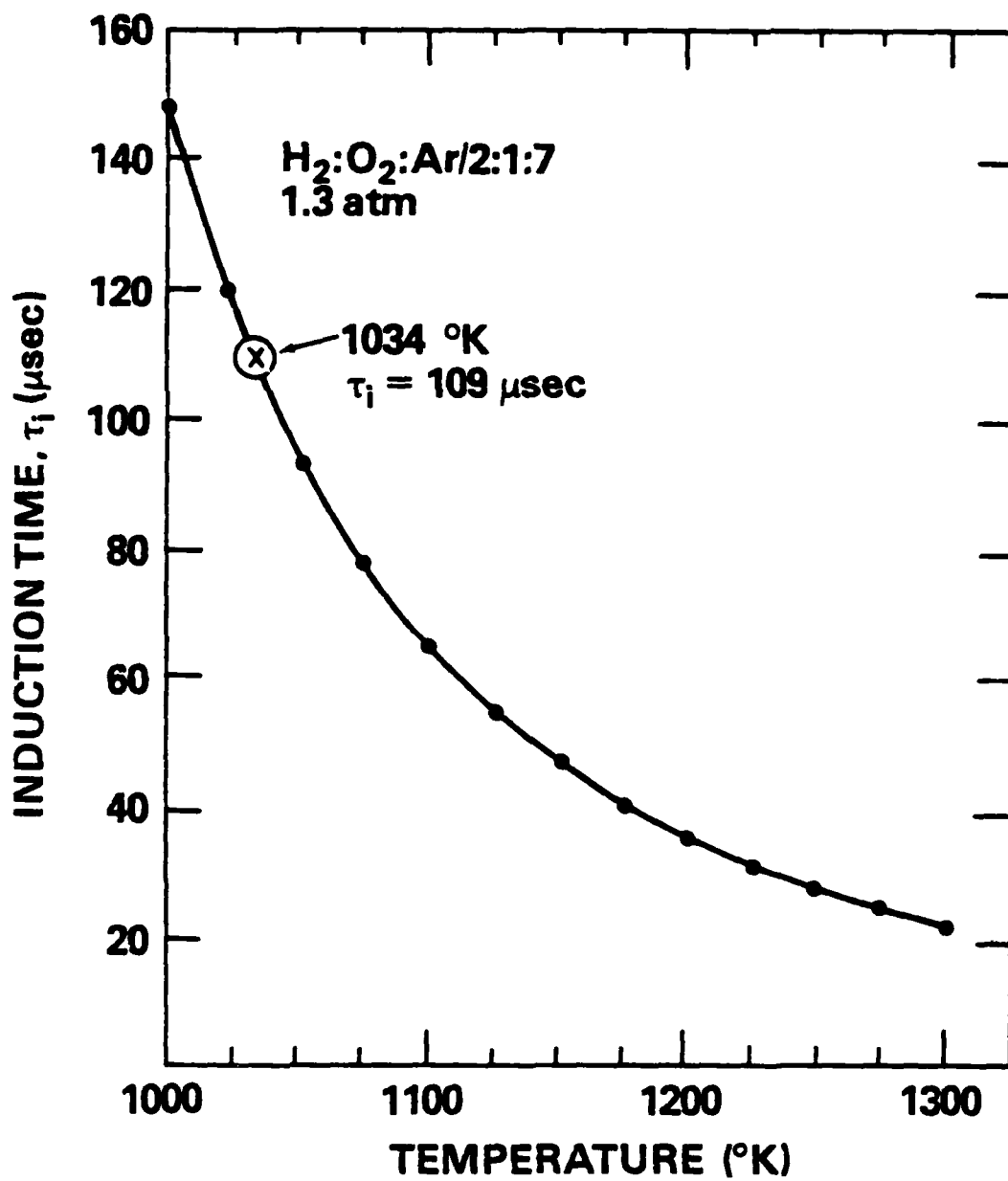


Fig. 5 — Calculations of chemical induction time as a function of temperature for the strong ignition case

1×10^4 cm/sec and then settles quickly to a very small value until the reaction wave starts and it jumps up again. Then the fluid velocity near the wall quickly decays again, and rises to a substantial value when the wave generated from the merging of the shock and reaction wave reaches the wall.

Figure 6 shows a tracing of the maximum system pressure and the wall velocity from the computer-generated output. There we see that the time calculated for the formation of the reaction wave is in good agreement with the experiment. There is apparent disagreement between the calculation and experiment in the individual times calculated for merging of the shock and reaction wave and the reflection of this wave from the wall, although the sum of these numbers is very close to that determined experimentally. In fact, there is some ambiguity (perhaps five microseconds) in determining these quantities from the original schlieren photograph.

Since the overall behavior of the simulation appears to agree well with the experiment, we look now at the results in more detail. Figure 7 shows the temperature and pressure of the reaction-wave before it merges with the reflected shock front. It looks like a detonation propagating into the shocked mixture. In fact it has become a detonation at about 35 μ sec after the reaction wave starts, as seen in Figure 8. Figure 8 shows the positions of the shock front, reaction wave, and merged wave and the contact discontinuity formed as the waves merge as a function of time. The reaction wave starts out slowly and then accelerates to a detonation travelling at a velocity which is 2% less than the Chapman-Jouet velocity and about 15% greater than the experimental velocity. After it merges with the reflected shock front, it decelerates relative

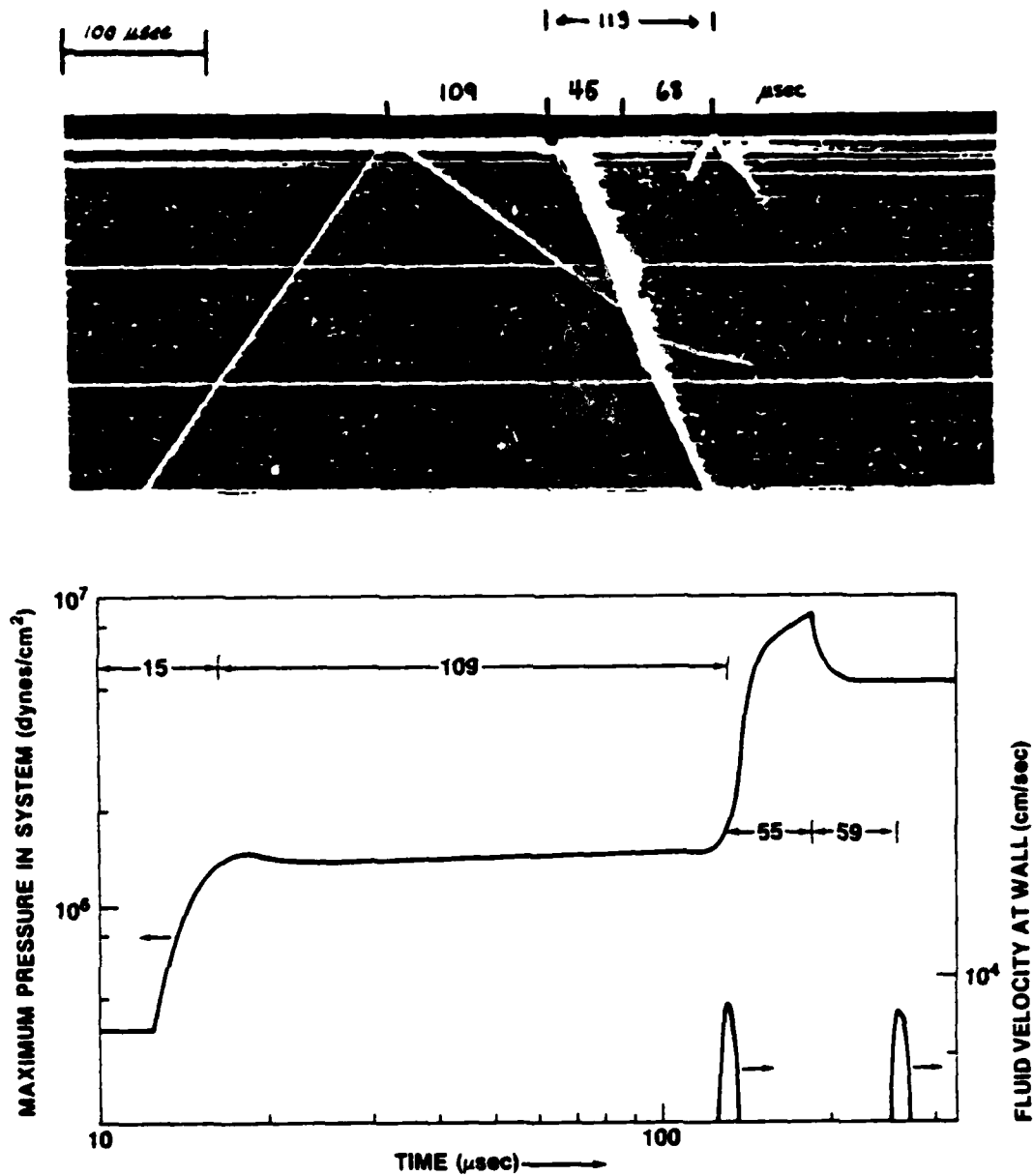


Fig. 6 — Comparison of calculation and experiment for the string ignition case. Top panel: schlieren photograph with relative times marked. Bottom panel: calculations of maximum pressure in the system and fluid velocity at 1 mm from the wall as a function of time with relative times marked.

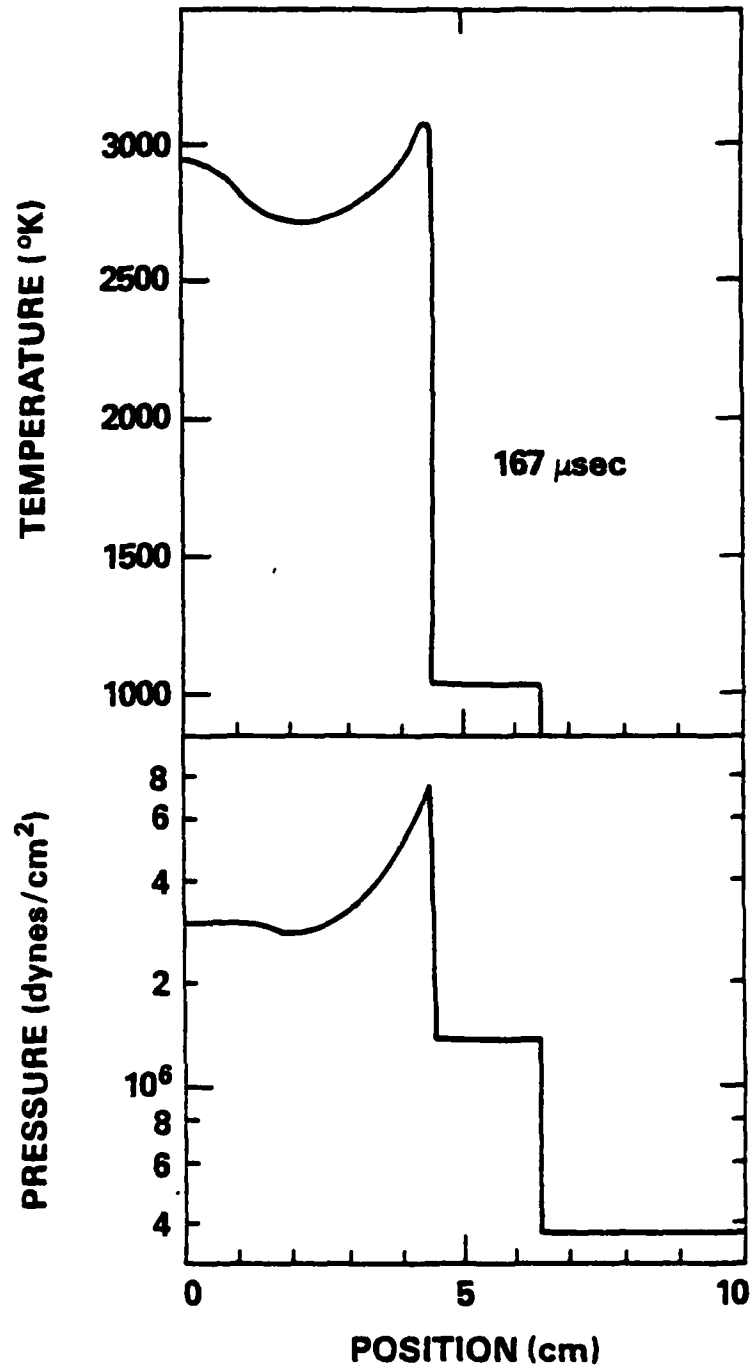


Fig. 7 — Temperature and pressure as a function of position for the strong ignition case

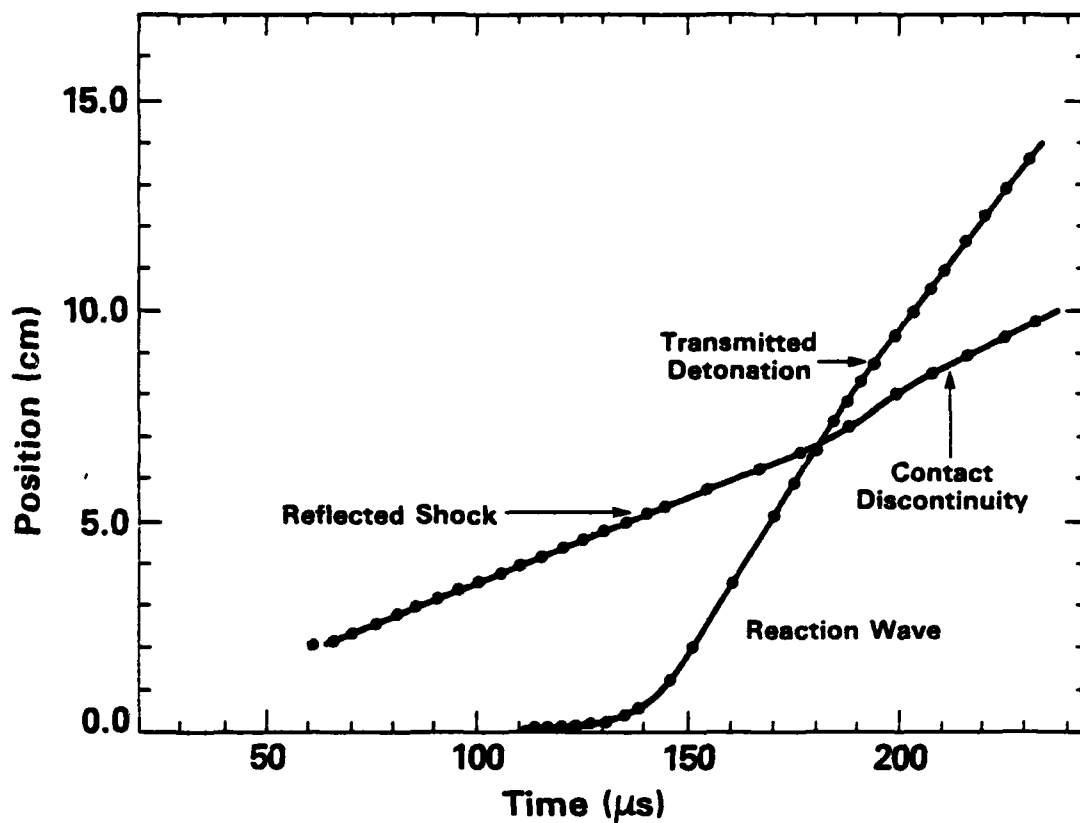


Fig. 8 — Calculated position of the reflected shock front reaction wave, transmitted detonation and contact discontinuity as a function of time for the strong ignition case

to laboratory coordinates due to the incoming incident shock flow. It moves at a velocity which is about 13% less than the Chapman-Jouget velocity and about 6% greater than the observed experimentally. The contact discontinuity formed when the waves merge moves forward more slowly, at the fluid velocity. Figure 9 shows the temperature profiles after the waves have merged for calculations using two different grid resolutions, indicating that the calculations have converged numerically.

Finally, Figure 10 shows the calculated number density of OH at a distance of 1 mm from the reflecting wall. In the experiment shown in Figure 2, OH was first detected by the absorption experiment 85 μsec after shock reflection. Thus we see from the graph that the number density at this time is about $2 \times 10^3 \text{ cm}^{-3}$. The observed emission delay time for OH was 126 μsec ; at this time in the calculation the OH number density is approximately 10^{17} cm^{-3} .

We conclude then that for this case studied, the agreement between the experiment and the simulation is remarkably good. This is especially gratifying since it is a direct test of both the individual components of the calculation and of the procedure used to couple the chemical kinetics and the convective transport. The calculation is so good that one is tempted to use it to calibrate the experimental diagnostics.

V. Simulation of a Weak Ignition Case

Historically the weak ignition regime in reflected shock experiments is one in which ignition is unpredictable. A neat, clean, distinct reaction wave, as we have seen above, does not appear at reproducible times at the reflecting wall in a shock tube experiment. We began our study of the experiment represented by Figure 3 by calculating induction times as a

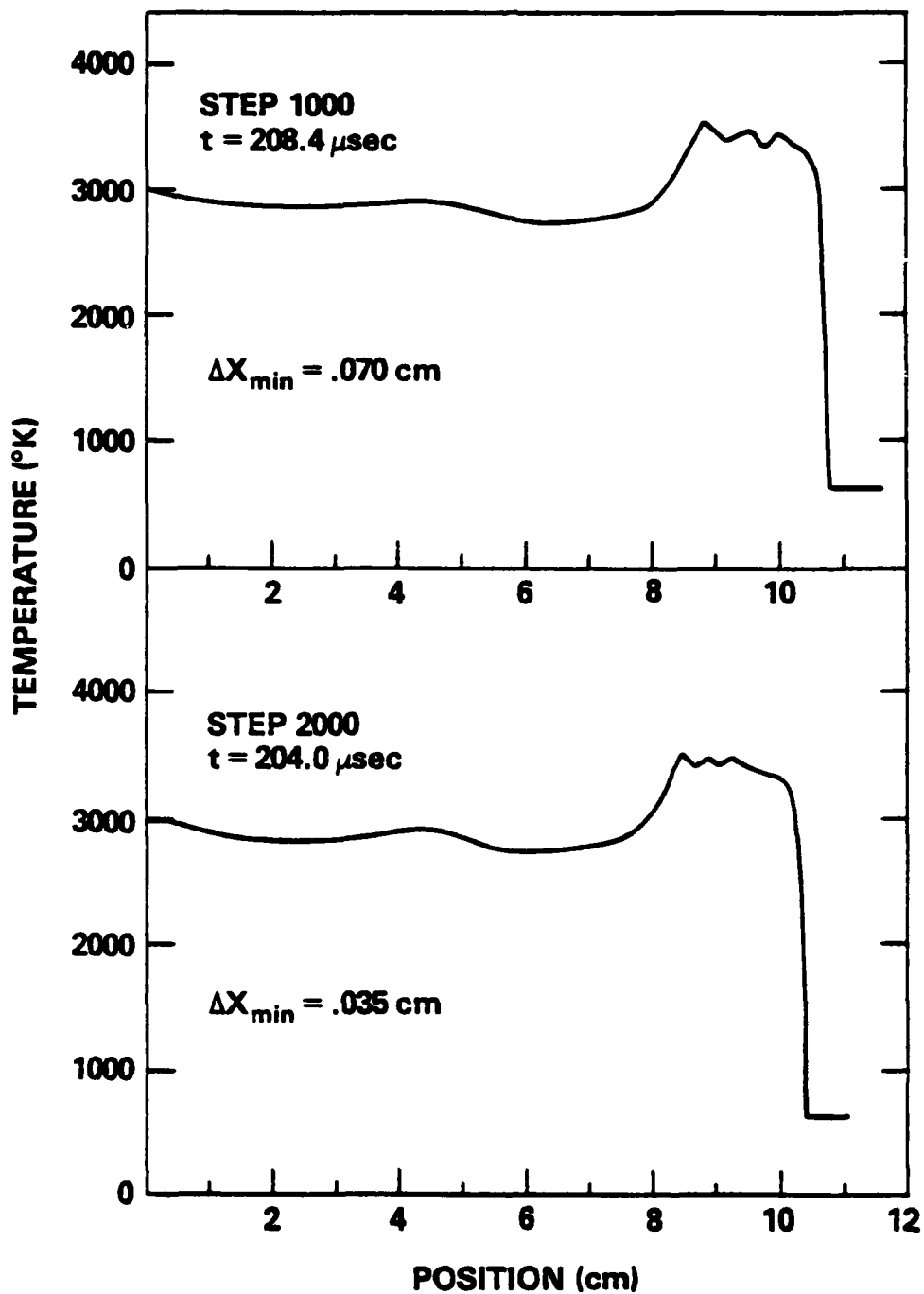


Fig. 9 — Resolution test of the calculated temperature as a function of position at a time after the merging of reaction wave and shock front

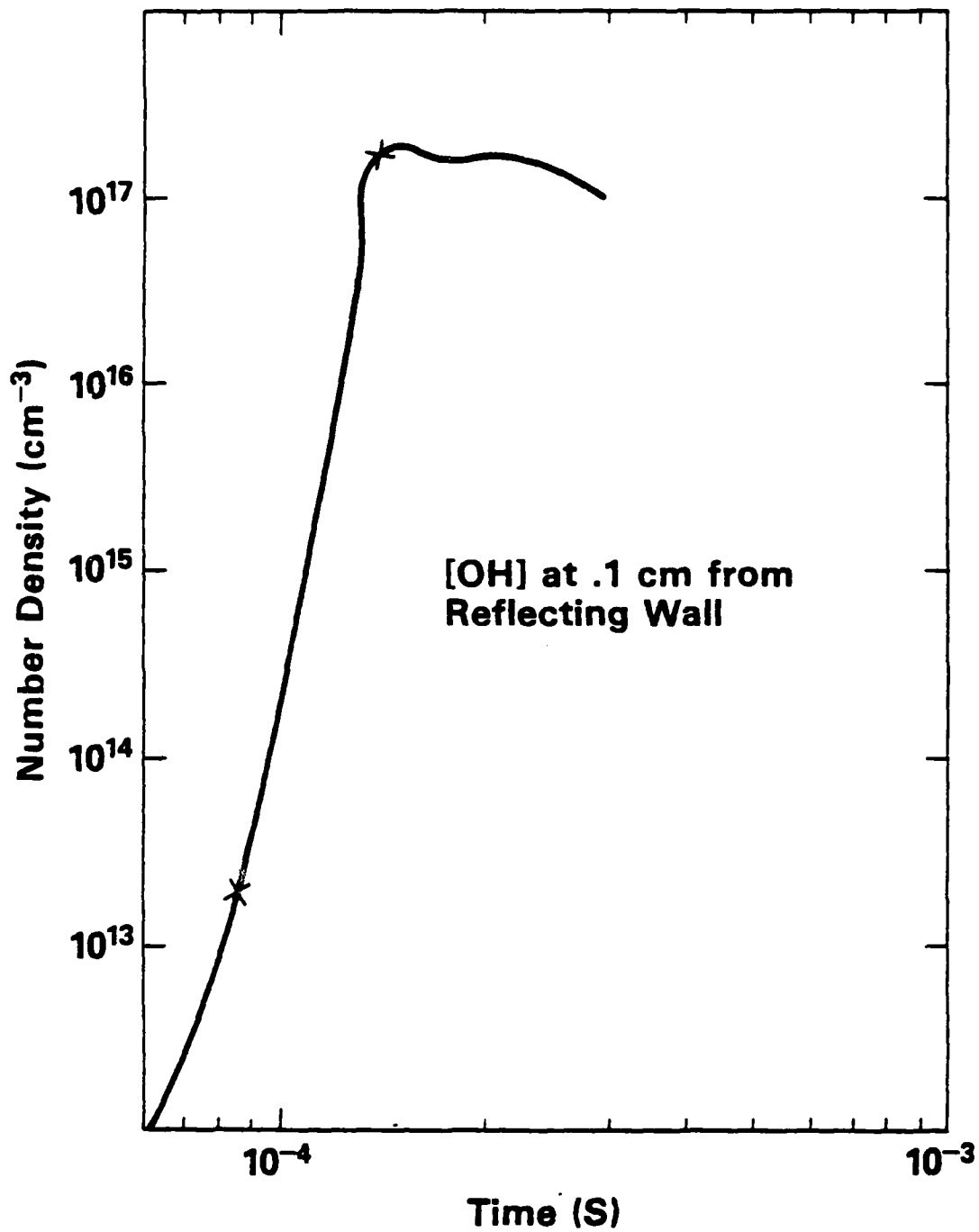


Fig. 10 — Calculated number density of OH as a function of time 1 mm from the reflecting wall for the strong ignition case

function of temperature for the conditions behind reflected shocks given in Table II. By analogy with the strong ignition case, in the ideal experiment and calculation the reaction wave should start at the reflecting wall about 3000 μ sec after shock reflection. In fact, the particular experiment shown in Figure 3 indicates that the reaction wave is first observed 726 μ sec after reflection, about a factor of four too soon. We further observe that the change in induction time with temperature is much greater in Figure 11 than in Figure 5.

While numerical simulations extending past 3000 μ sec and several meters are possible, we felt that we could learn just as much at lower cost by increasing the reflected shock temperature but remaining in the same general vicinity of pressure and temperature shown in Figure 11. Thus we simulated a case for which the temperature and pressure behind the reflected shock are 1000 K and 3.72 atm instead of 972 K and 3.4 atm for the same $H_2:O_2:Ar/8:2:90$ mixture. The calculated induction time for this mixture is ~ 1550 μ sec.

Figure 12 shows the position of the reflected shock front, reaction wave, and the transmitted detonation as a function of time for this case. In this calculation, the reaction wave is defined as that place where the ratio of OH to Argon becomes significant and energy has just begun to be released. We note first that the incident shock reflection occurs at ~ 100 μ s into the calculation. The first indication of energy release occurs at the time 850 μ s which is 750 μ s after shock reflection. By 1120 μ s, it appears that a detonation has formed in the region behind the shock. Figure 13 shows profiles of temperature as a function of position for selected times during the period from 820 to 1220 μ s. We see that in

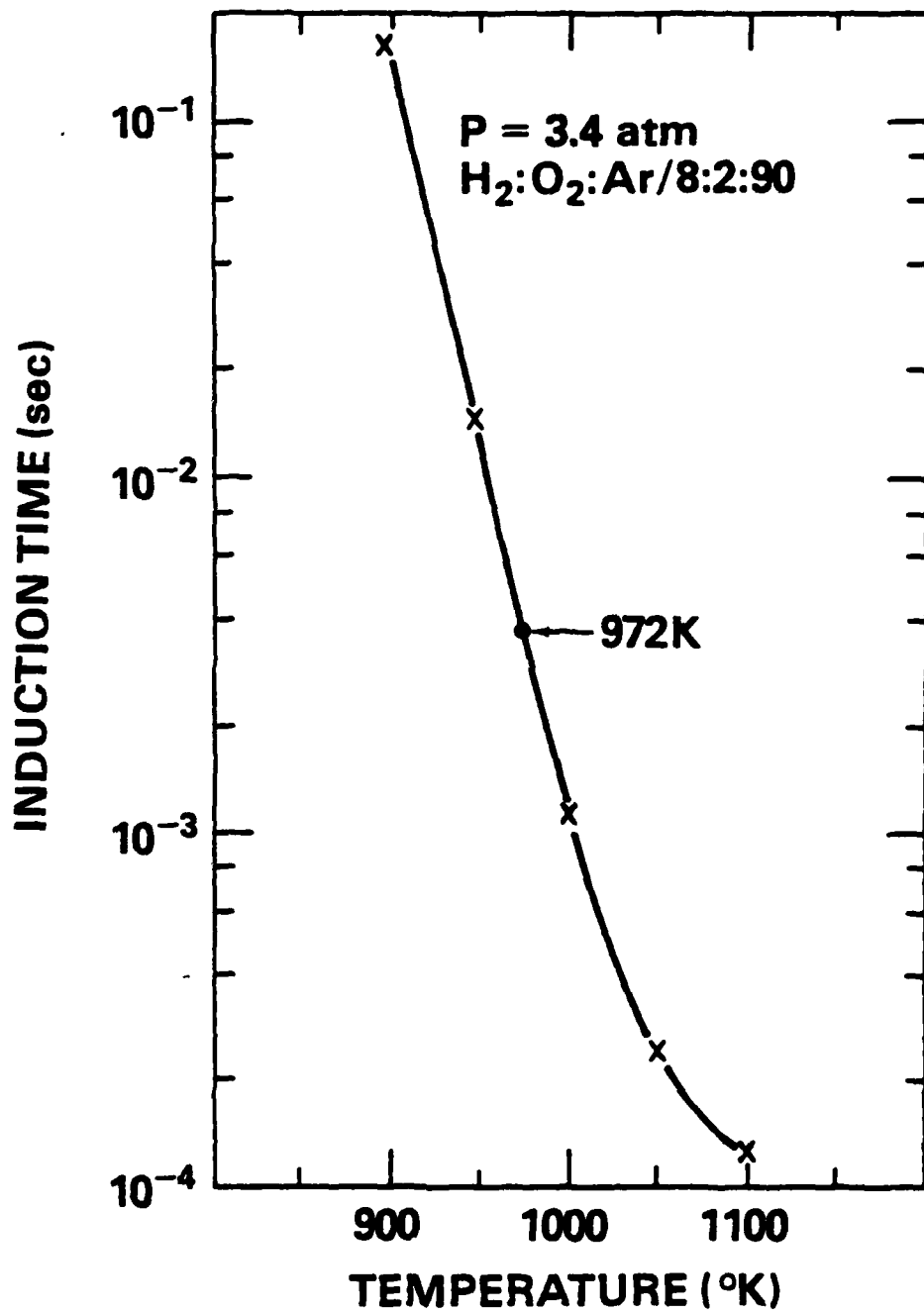


Fig. 11 — Calculations of the chemical induction time as a function of temperature for the weak ignition case

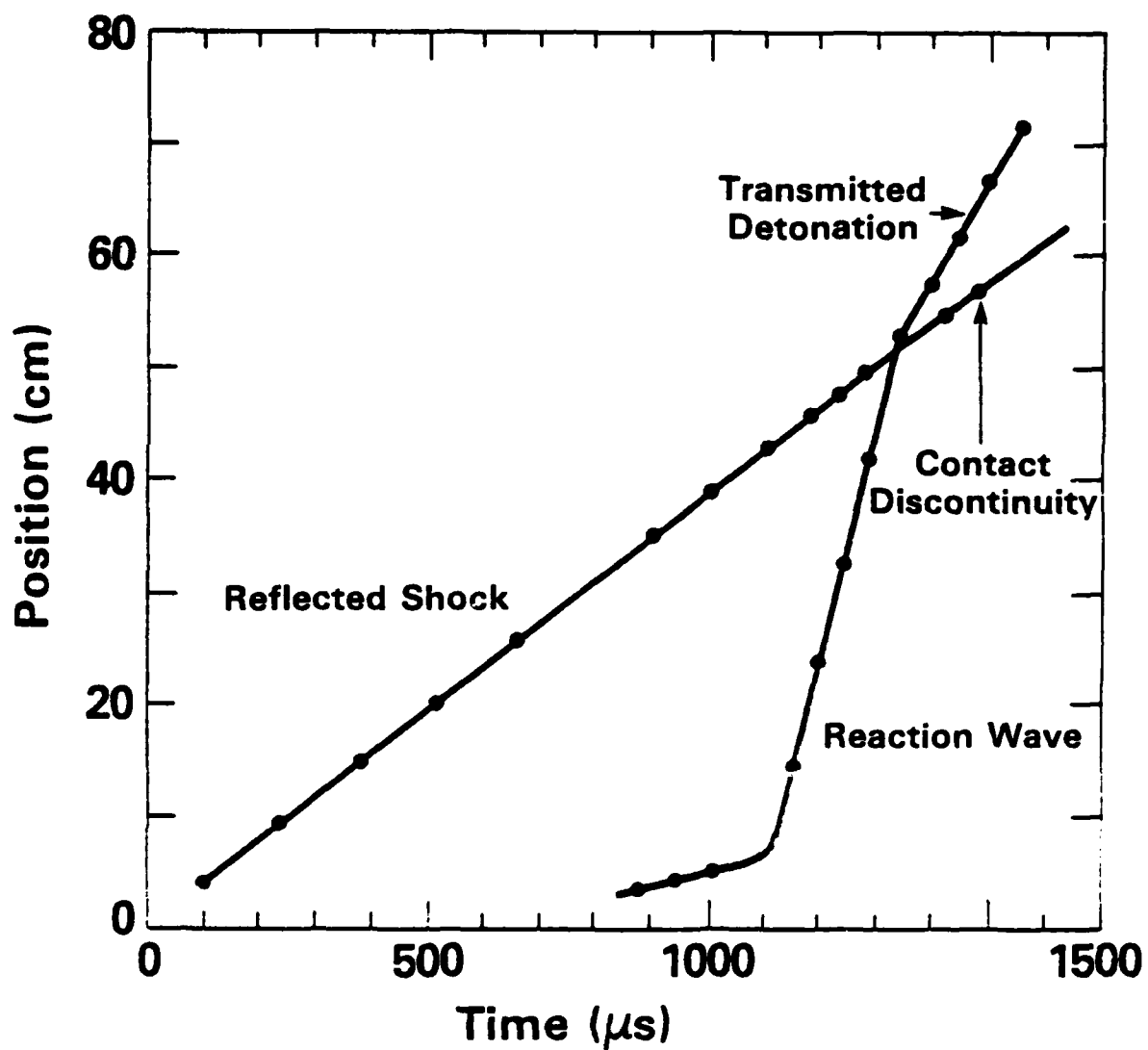


Fig. 12 — Calculated position of the reflected shock front, reaction wave, transmitted detonation, and contact discontinuity as a function of time for the weak ignition case

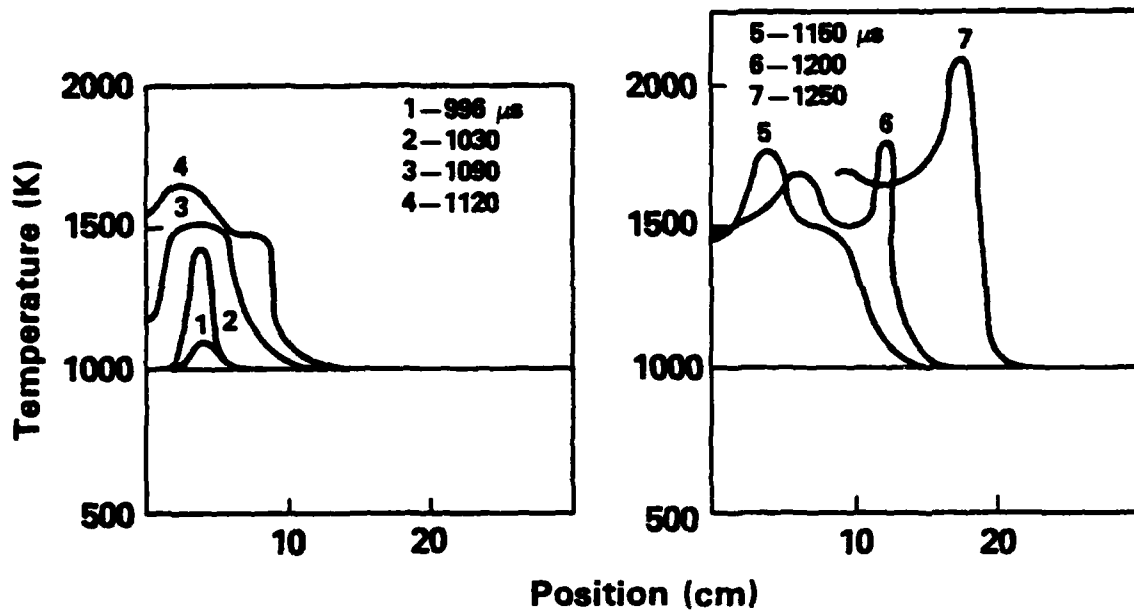


Fig. 13 — Calculated temperature as a function of position at selected times for the weak ignition case

fact ignition has not started at the wall in the calculation, but at a location about 3.5 cm from the wall.

A close look at the calculation indicates that there are effects present which may cause the results to deviate from ideality. One effect is numerical "clipping" [20] which causes the temperatures near the reflected wall to fluctuate slightly from the ideal solution. This is a small effect, causing a perturbation of a few degrees (about 0.05%) for an extent of about five cells. Such a temperature perturbation had a negligible effect on the strong ignition problem (Figure 5) but had a noticeable effect on mild ignition (Figure 11). Another effect observed in the calculation is the presence of small but finite velocities behind the reflected shock during the reflection period. As shown in Figures 6 and 14, these velocities start out at fairly large amplitudes ($\sim 5 \times 10^3$ cm/s) and then die out.

Thus, although this is a one-dimensional calculation and we therefore cannot resolve transverse perturbations and boundary layers, we find that in the weak ignition case the system is extremely sensitive to non-idealities and small perturbations. We have thus introduced essentially the same perturbation in both the strong and the weak ignition calculations. In the strong ignition case we have obtained quantitative agreement with the experiment and in the weak ignition case we obtain agreement qualitatively similar to that observed experimentally. It is also clear that the ignition variability in the weak ignition cases is adequately reflected in the much steeper induction time versus temperature curve of Figure 11 relative to Figure 5. In the weak cases, fluctuation velocities of 5×10^3 cm/sec correspond to temperature fluctuations of 10°K or greater. These 1% fluctuations correspond to 100% variations in the extremely sensitive chemical induction time.

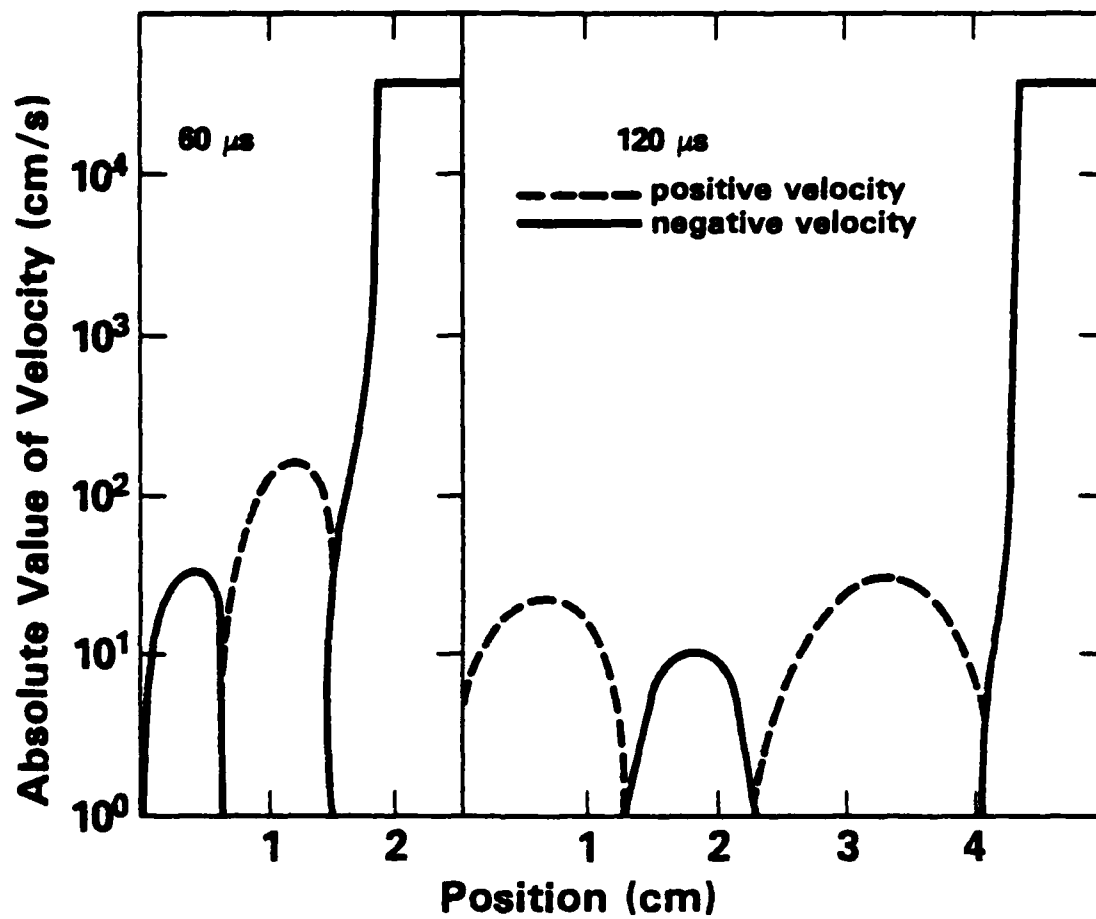


Fig. 14 — Calculate values of the fluid velocity as a function of position at two times after shock reflection

VI. Discussion

There are a number of factors that might help explain the behavior observed in a weak ignition experiments. We know that the fluid in the shock tube behind both an incident and reflected shocks is not uniform. Boundary layers and transverse waves exist which perturb the conditions on the centerline. Nonuniformities in the incident shock may cause it to hit the reflecting wall at different times at each position in the wall. Thus shock reflection and focusing effects may cause uneven ignition. In the case of reflected shocks, there may be reflections arising from the interaction of the reflected wave and the contact discontinuity formed at the onset of the experiment. Thus when the reflected wave travels long times and distances before the reaction wave starts, there is more chance for the medium to be perturbed. This is especially true when, as we see in Figure 11, the medium is particularly sensitive to perturbations.

We have seen that there are deviations from ideality in the one-dimensional calculations used to model both weak and strong ignition. Large oscillating fluid velocities appear near the wall when the shock reflects. Even though these are quickly damped, there is always a residual, nonzero velocity behind the reflected shock. There is also a deviation in the temperature from exactly 1000 K at the wall, the temperature may be 995 K for the first few cells. This latter effect mimics the effects of heat loss to a wall due to thermal conduction. In the case of mild ignition, where the induction time is sensitive to perturbations, we expect that these deviations from non-ideality might have a noticeable effect on our answers.

In the companion paper which follows this we have analyzed the hydrogen-oxygen system with respect to the sensitivity of the induction time to sound wave and entropy wave perturbations. This had led to the development of a model which couples the chemical kinetic sensitivity with the hydrodynamic fluctuations to quantify the system's behavior. This model clarifies much of the weak ignition variability, and it provides a scientific basis for an improved global induction time model [31,32].

ACKNOWLEDGEMENTS

The authors would like to acknowledge the encouragement of Prof. Roger Stehlow. This work was supported by the Naval Research Laboratory through the Office of Naval Research and the Naval Material Command.

REFERENCES

1. Shepherd, W. C. F., Third Symposium (International) on Combustion, The Williams and Wilkens Co., Baltimore, 1949, p. 301.
2. Berets, D. J., Greene, E. F., Kistiakowsky, G. B., J. Am. Chem. Soc. 72, 1080, (1950).
3. Fay, J. A., Fourth Symposium (International) on Combustion, The Williams and Wilkens Co., Baltimore, 1953, p. 501.
4. Steinberg, M. and Kaskan, W. E., Fifth Symposium (International) on Combustion, Reinhold, New York, 1955, p. 664.
5. Strehlow, R. A., and Cohen, A., Phys. Fluids 5, 97 (1962).
6. Strehlow, R. A., and Dyner, H. B., AIAA Journal 1, 591 (1963).
7. Gilbert, R. B., and Strehlow, R. A., AIAA Journal 4, 1777 (1966).
8. Soloukhin, R. I., Shock Waves and Detonations in Gases, Moscow, FM, 1963; also Doklady Akad. Nauk. SSSR 122, 1039 (1958).
9. Zaitsev, S. G., and Soloukhin, R. I., Eighth Symposium (International) on Combustion, The Williams and Wilkens Co., Baltimore, 1962, p. 335.
10. Voevodsky, V. V., and Soloukhin, R. I., Tenth Symposium (International) on Combustion, The Combustion Institute, Pittsburgh, PA., 1965, p. 279.
11. Meyer, J. W., and Oppenheim, A. K., Thirteenth Symposium (International) on Combustion, The Combustion Institute, Pittsburgh, PA., 1970, p. 1153.
12. Meyer, J. W., and Oppenheim, A. K., Comb. and Flame, 17, 65 (1971).
13. Meyer, J. W., Cohen, K. M., and Oppenheim, A. K., Comb. Sci. Tech., 8, 185 (1973).
14. Zajac, L. J., and Oppenheim, A. K., AIAA Journal 9, 545, (1971).
15. Van Tiggelen, P. J., Comb. Sci. and Tech., 1, 225 (1969).
16. Borisov, A. A., Acta Astronautica, 1, 909 (1974).

17. Cohen, A. and Larsen, J., Explosive Mechanism of the H₂-O₂ Reaction near the Second Ignition Limit, B. R. L. Rpt. No. 1386, Ballistics Research Laboratories, Aberdeen, Maryland, 1967.
18. Oran, E. S., and Boris, J. P., Prog. Energy Combustion Science, 7:1-72 (1981).
19. Jones, W. W., and Boris, J. P., FLAME - A Slow-Flow Combustion Model, NRL Memorandum Report 3970.
20. Boris, J. P., and Book, D. L.: Methods in Computational Physics, Vol. 16, p. 85, Academic Press, 1976.
21. Boris, J. P.: Flux-Corrected Transport Modules for Solving Generalized Continuity Equations, Naval Research Laboratory Memorandum Report 3237, 1976.
22. Young, T. R., and Boris, J. P., J. Phys. Chem. 81, 2424-2427 (1977).
23. Young, T. R., CHEMEQ, A Subroutine for Solving Stiff Ordinary Differential Equations, N. R. L. Memorandum Report 4091, Naval Research Laboratory, Washington, D.C., 1980.
24. Oran, E. S., Young, T. R., and Boris, J. P.: Seventeenth Symposium (International) on Combustion, p. 43, The Combustion Institute, 1978.
25. Oran, E. S., and Boris, J. P., presented at the 7th International Colloquium on Gas Dynamics of Explosions and Reactive Systems, Göttingen, 1979, to appear in Prog. in Astronautics and Aeronautics, 1981.
26. Kailasanath, K., Oran, E. S., Boris, J. P., A Theoretical Study of the Ignition of Premixed Gases, submitted to Comb. Flame.
27. Burks, T. L., and Oran, E. S., A Computational Study of the Chemical Kinetics of Hydrogen Combustion, N.R.L. Memorandum Report 4446, Naval Research Laboratory, Washington, D.C., 1980.
28. Indritz, D., Boris, J., Carhart, H., Oran, E., Sheinson, R., Williams, F., and Young, T., Computation of Hydrogen-Oxygen Flammability Limits, submitted to Comb. Flame.

29. Stull, D. R., and Prophet, H., JANAF Thermochemical Tables, National Standard Reference Data Series, U.S. National Bureau of Standards, No. 37, 2nd Ed., Gaithersburg, Maryland, 1971.
30. Oran, E. S., and Boris, J. P., Numerical Simulation of Reaction Waves to appear in Proceedings of the First International Specialists Meeting, Bordeaux, 1981.
31. Oran, E. S., Boris, J. P., Young, T. R., Flanigan, M., Burks, T., and Picone, M., Eighteenth Symposium (International) on Combustion, The Combustion Institute, Pittsburgh, 1981.
32. Oran, E. S., Boris, J. P., Young, T. R., Simulations of Gas Phase Detonations, NRL Memo Report 4255, Naval Research Laboratory, Washington, D.C. 20375, 1980.
33. Baulch, D. L., Drysdale, D. C., Horne, D. G., and Lloyd, A. C., Evaluated Kinetic Data for High Temperature Reactions, Vol. 1, Butterworths, London, 1972.
34. Hampson, R. F., and Garvin, D., "Chemical Kinetic and Photochemical Data for Modelling of Atmospheric Chemistry," NBS Technical Note 866, National Bureau of Standards, Washington, D.C. (1975).
35. Cohen, N., and Westberg, K. R., "Data Sheets," The Aerospace Corporation, P.O. Box 92957, Los Angeles, California (1979).
36. Olson, D. B., and Gardiner, W. C., *J. Phy. Chem.*, 81, 2514 (1977).
37. Lloyd, A. C., *Int. J. Chem. Kinetics*, 6, 169 (1974).
38. Bahn, G. S., "Reaction Rate Compilation for H-O-N System," Gordon and Breach, New York, 1968.

**DATE
FILMED**

